Cement and Concrete Research 40 (2010) 1211–1225

Contents lists available at ScienceDirect

Cement and Concrete Research

journal homepage: http://ees.elsevier.com/CEMCON/default.asp

Sulfate ingress in Portland cement

Barbara Lothenbach [a,*], Benoît Bary [b], Patrick Le Bescop [b], Thomas Schmidt [a], Nikos Leterrier [c]

[a] Empa, Laboratory for Concrete & Construction Chemistry, Überlandstrasse 129, CH-8600 Dübendorf, Switzerland
[b] CEA, DEN, DPC, SCCME, Laboratory of Study of Concrete and Clay Behaviour, CEA Saclay, Bâtiment 158, 91191 Gif/Yvette Cedex, France
[c] CEA, DEN, DM2S, SFME, Laboratory of Simulation of Flows and Transport, CEA Saclay, Bâtiment 454, 91191 Gif/Yvette Cedex, France

ARTICLE INFO

Article history:
Received 24 November 2009
Accepted 19 April 2010

Keywords:
Sulfate
Limestone
Modelling
Thermodynamic
Transport

ABSTRACT

The interaction of mortar with sulfate solutions leads to a reaction front within the porous material and to expansion. Thermodynamic modelling coupled with transport codes was used to predict sulfate ingress. Alternatively, "pure" thermodynamic models – without consideration of transport – were used as a fast alternative to coupled models: they are more flexible and allow easy parameter variations but the results relate neither to distance nor to time. Both transport and pure thermodynamic modelling gave comparable results and were able to reproduce the changes observed in experiments. The calculated total volume of the solids did not exceed the initial volume of the paste indicating that not the overall volume restriction leads to the observed expansion but rather the formation of ettringite within the matrix and the development of crystallisation pressure in small pores. The calculations indicate that periodic changing of the Na_2SO_4 solution results in more intense degradation.

1. Introduction

Sulfates present in groundwater or soils surrounding a concrete structure pose a serious threat to its long-term durability. The interaction of cementitious materials with solutions containing sulfate leads to the formation of a reaction front within the porous material. The formation of ettringite and also of gypsum in the presence of higher sulfate concentrations have been observed near the material surface [1,2]. Significant damage due to sulfate interaction can result in the structural breakdown of the concrete structure.

To test the "sulfate resistance" of a specific cement, mortar or concrete, samples are generally immersed for a few weeks in concentrated Na_2SO_4-solutions and the mass and length gain is monitored as a function of time. High sulfate concentrations, as used in such tests, lead to the precipitation of gypsum, while lower sulfate concentrations, as present under field conditions, lead to no or only very little gypsum precipitation [1,3]. The mortar samples show strongly differing expansion and mass gain depending on their composition, on the reaction solution and the temperature. Further factors influencing the expansion are the sample geometry, the amount of solution, the frequency of the exchange of the solutions [4] and the absence or presence of CO_2 in the interacting solution [5]. Considering all these factors, it is not surprising that the tests carried out in different laboratories show large variations [6,7]. In addition, the correlation of the test results with expansion and deterioration under field conditions is poorly understood.

Thermodynamic modelling coupled with transport codes can be used to predict which hydrate phases are formed under which conditions and deepen our understanding of the processes that take place during sulfate interaction (see e.g. [8]). Transport models are able to predict the changes induced by sulfate ingress as a function of time and ingress depth; to do this, different transport parameters have to be estimated. If molecular diffusion phenomena through saturated porosity are considered, then the diffusivity of all ionic species has to be known as a function of porosity.

Different approaches may be used for performing chemical–transport simulations of the degradation of concrete materials (e.g. [8–13]). Simplified approaches have been proposed in the case of leaching, where only calcium ions are supposed to govern the main chemical reactions (e.g. [9]), or in the case of carbonation and sulfate attack where an additional species (either carbonates of sulfates) is necessary to describe such reactions [14,15]. More advanced approaches capable of treating multi-species reactive transport problems are also available [12,13], where the current chemical equilibrium state is obtained locally by means of a chemical equilibrium code (coupled chemical–transport models). Such numerical tools turn out to be essential when the degraded states of the material have to be precisely predicted in terms of the time evolution of volume fraction of the various hydrated products dissolved or precipitated at each point of the material. These tools are also crucial in the case of complex aggressive solutions containing different ionic species (this includes the alkalis initially present in the pore solution which affect all ion concentrations), which generally cannot be directly

* Corresponding author.
E-mail address: barbara.lothenbach@empa.ch (B. Lothenbach).

0008-8846/$ – see front matter © 2010 Elsevier Ltd. All rights reserved.
doi:10.1016/j.cemconres.2010.04.004

considered by simplified approaches involving only a limited number of species (e.g. [15,16]).

Alternatively, "pure" thermodynamic models – without consideration of transport – can be a fast and easily available alternative to coupled chemical–transport models. "Pure" thermodynamic models are generally more flexible and allow easy and fast parameter variations which makes systematic variations of the input parameters such as the composition of the solid or the liquid phase unproblematic. The ingress of sulfates can be mimicked by assuming that solid phases are in contact with different quantities of the Na_2SO_4 solution.

In this paper the changes caused by the presence of high sulfate concentrations, as typical for test conditions, are compared to the changes observed in the presence of lower sulfate concentrations, more representative of real groundwater conditions. The evolution of the composition of the solid and liquid phases exposed to Na_2SO_4 solutions is calculated by "pure" thermodynamic modelling as well as by a coupled chemical–transport model. The results are compared with each other as well as with experimental data.

2. Materials and methods

All experiments were carried out using a laboratory produced Portland cement, comparable to CEM I 42.5 N, which contained only 0.2 % of CO_2 (Table 1). Laboratory ground clinker has been homogenized with 4.7 weight% of gypsum (Fluka purum p.a.). The chemical compositions of the materials as given in Table 1 were determined by X-ray fluorescence (XRF), sulfur and carbonate with a LECO C/S analyzer, and free lime according to Franke [17].

Mortar prisms 4×16×23 cm were prepared according to EN 196-1 with a w/c of 0.5. The mortar samples were cured for 28 days in saturated limewater at 20 °C, then mortar prisms of a size 1×4×16 cm were cut and exposed to solutions containing 4 or 44 g/L Na_2SO_4 at 20 °C. Control samples were exposed to limewater. The liquid/solid — volume ratio of the batches was 4 to 1. The sulfate solutions were changed after 7, 14, 28, 56, 91, 180, 270 and 365 days.

The mortar samples were examined by scanning electron microscopy SEM (Philips ESEM FEG XL 30) using backscattered electron images and energy dispersive X-ray spectroscopy (EDS). Sample preparation included drying, impregnation with epoxy resin, cutting, polishing and coating with carbon. The EDS analysis was done using a Li/Si crystal detector and an accelerating voltage of 15 kV. The sulfate uptake and the calcium leaching was determined on polished samples as the SO_3 and CaO content by mass cement paste using area scans (100×100 µm).

Table 1
Composition of the Portland cement used.

Chemical analysis [g/100 g]		Normative phase composition [g/100 g]	
CaO	63.7	Alite	62.5
SiO_2	20.1	Belite	10.5
Al_2O_3	4.4	Aluminate	7.1
Fe_2O_3	2.7	Ferrite	8.2
CaO (free)	0.85	CaO (free)	0.85
MgO	1.6	$CaCO_3$	0.45
K_2O	0.86	$CaSO_4 \cdot 2H_2O$	4.7
Na_2O	0.15	K_2SO_4 [a]	1.3
CO_2	0.20	Na_2SO_4 [a]	0.14
SO_3	2.90	MgO [b]	1.6
$K_2O_{soluble}$ [a]	0.72	K_2O [b]	0.14
$Na_2O_{soluble}$ [a]	0.06	Na_2O [b]	0.09
Ignition loss	1.2	SO_3 [b]	0.03
Blaine surface area [m^2/kg]	350		

[a] Readily soluble alkalis calculated from the concentrations of alkalis measured in the solution after 5 min of agitation at a w/c of 10; present as alkali sulfates.
[b] Present as solid solution in the clinker phases.

3. Modelling

3.1. Data used in both approaches

"Pure" thermodynamic modelling was carried out using GEMS ([18], for further details see Section 3.2 below), while the coupled chemical–transport modelling used the platform ALLIANCES (see Section 3.3).

In both cases the same input parameters and the same thermodynamic database were used. The thermodynamic data for aqueous species as well as for many solids were taken from the PSI-GEMS thermodynamic database [19,20]. Solubility products for cement minerals including ettringite, different AFm phases, hydrogarnet, C–S–H and hydrotalcite were taken from the recent compilations of Lothenbach et al. (cemdata2007 in [21]).

3.1.1. Porosity

Based on the calculated volumes of the solid phases the theoretical porosity of the mortar samples were calculated according to

$$\phi_t = \frac{V_{cement,0} + V_{solution,0} - V_{cement,h} - V_{hydrates,h}}{V_{cement,0} + V_{solution,0} + V_{aggregate}} \quad (1)$$

where ϕ_t is the (total) porosity in %, V_{cement} the volume of the unhydrated fraction of cements, V_0 is the volume in cm^3 before hydration, and V_h the volume after hydration and/or sulfate ingress. $V_{solution}$ and $V_{aggregate}$ refer to the volume of the pore solution and aggregate in the material, respectively. The calculated "total" porosity corresponds to the difference between the initial volume of the system before the start of hydration and the volume of the hydrates and the unreacted cement after hydration and/or interaction with the sulfate containing solutions. This total porosity corresponds roughly to the sum of "gel" and "capillary" porosity but does not include the changes in porosity created by air voids, cracks, or chemical shrinkage.

The capillary porosity was calculated based on the total porosity by subtracting the volume of the gel pores [22,23]. The gel porosity associated with C–S–H was computed from the difference between the molecular volume of C–S–H globules $C_{1.7}SH_{2.1}$ (78 cm^3/mol; cf Table 2 and [21]) and the molecular volume of water saturated C–S–H gel, nominally $C_{1.67}SH_4$ (113 cm^3/mol [24]). The approach used in this paper to calculate the volume fraction and the porosity is similar to the approach described by Parrot et al. [22,25,26]. The main difference, however, is that the composition of the hydrate assemblage is not derived from a priori assumptions which solids are present but the hydrate assemblage is calculated directly from fundamental thermodynamic data.

3.1.2. Degree of hydration

The degree of hydration of the cement, when the samples were immersed in the Na_2SO_4 solutions, was estimated based on an empirical model that describes the dissolution of the clinker as a function of time [25,27]. The composition of the solid phase as a function of time is calculated based on (i) the composition of the cement as given in Table 1, (ii) the calculated degree of the dissolution of the clinkers and (iii) thermodynamic equilibrium calculations (for details see [27,28]).

3.2. "Pure" thermodynamic modelling

The different conditions which may be present in a mortar sample immersed in Na_2SO_4 solutions can be expressed as the ratio of Na_2SO_4 solution/mortar [3,4] assuming that the core of the sample is not or hardly affected by the presence of Na_2SO_4 while the outermost layer is in contact with a large amount of Na_2SO_4 solution. Such a modelling approach has the advantage that the calculations are very fast and flexible as no transport equations have to be considered, but has the disadvantage that the calculated data relate neither to time nor to distance and that effects such as back-diffusion cannot be considered.

Table 2
Standard thermodynamic properties at 25 °C for solids present in cements: Thermodynamic data "cemdata2007" taken from Lothenbach et al. [21], supplied with data from Thoenen et al. [19].

	log K_{s0}[a]	$\Delta_f G°$ [kJ/mol]	V° [cm^3/mol]
(Al-)ettringite	−44.9	−15,205.94	707
Tricarboaluminate	−46.5	−14,565.64	650
Fe-ettringite	−44.0	−14,282.36	717
C_3AH_6	−20.84	−5010.09	150
C_3FH_6	−25.16	−4116.29	155
C_4AH_{13}	−25.40	−7326.56	274
C_2AH_8	−13.56	−4812.76	184
C_4AsH_{12}	−29.26	−7778.50	309
$C_4A\overline{C}H_{11}$	−31.47	−7337.46	262
$C_4A\overline{C}_{0.5}H_{12}$	−29.13	−7335.97	285
C_2ASH_8	−19.70	−5705.15	216
C_4FH_{13}	−29.4	−6430.94	286
C_2FH_8	−17.6	−3917.38	194
C_4FsH_{12}	−33.2	−6882.55	322
$C_4F\overline{C}H_{12}$	−35.5	−6679.20	290
$C_4F\overline{C}_{0.5}H_{12}$	−33.1	−6440.19	296
C_2FSH_8	−23.7	−4809.53	227
M_4AH_{10}	−56.02	−6394.56	220
M_4AcH_9	−51.14	−6580.15	220
M_4FH_{10}	−60.0	−5498.84	232
$C_{1.67}SH_{2.1}$(jen.)	−13.17	−2480.81	78[b]
$C_{1.67}SH_4$(jen.)	−13.17	−2931.46	113[b]
$C_{0.83}SH_{1.3}$(tob.)	−8.0	−1744.36	59
Portlandite	−5.20	−897.01	33
$SiO_{2,am}$	1.476	−848.90	29
H_2O	−14.00	−237.18	18
Gypsum	−4.58	−1797.76	75
Anhydrite	−4.36	−1322.12	46
Syngenite[c]	−7.20	−2884.91	128
Calcite	−8.48	−1129.18	37
Brucite	−11.16	−832.23	25
$Al(OH)_3$(am)	0.24	−1143.21	32
$Fe(OH)_3$(mic)	−4.60	−711.61	34
C_3S		−2784.33	73
C_2S		−2193.21	52
C_3A		−3382.35	89
C_4AF		−4786.50	130

[a] All solubility products refer to the solubility with respect to the species $Al(OH)_4^-$, $Fe(OH)_4^-$, $SiO(OH)_3^-$, OH^-, H_2O, Ca^{2+}, Mg^{2+}, CO_3^{2-} or SO_4^{2-}.
[b] To calculate the gel porosity a volume of $C_{1.67}SH_4$ of 113 cm^3/mol was used as calculated from the density given in Thomas and Jennings [24].
[c] Solubility data for syngenite from [28] and volume calculated from density data from [48].

Thermodynamic modelling was carried out using the Gibbs free energy minimization program GEMS [18]. GEMS is a broad-purpose geochemical modelling code which computes equilibrium phase assemblage and speciation in a complex chemical system from its total bulk elemental composition. Chemical interactions involving solids, solid solutions, and aqueous electrolytes are considered simultaneously. The speciation of the dissolved species as well as the kind and amount of solids precipitated are calculated.

3.3. Coupled chemical–transport modelling

3.3.1. General description

The ALLIANCES platform couples the chemical code CHESS [29] with the finite volume software CAST3M and solves multi-species reactive transport problems such as the degradation of cement-based materials. Such coupled problems may take the following form:

$$\begin{cases} \dfrac{\partial(\phi_t C_i)}{\partial t} = \mathcal{T}(\phi_t, \phi_m, C_i) \\ (C_i, C_m) = \mathcal{C}_{0i}(C_i) \\ \phi_t = \left(1 + \sum_{m=1}^{M} \overline{V}_m C_m\right)^{-1}, \ \forall i \in \{1,\ldots,N\}, \forall m \in \{1,\ldots,M_i\} \end{cases} \quad (2)$$

where ϕ_t and C_i denote the porosity and the concentrations of the aqueous species; ϕ_m, C_m and ∇_m designate the volume fractions, the concentrations and the molar volume of the mineral m, respectively. The material initially contains M_i homogeneous mineral phases and N aqueous species, most of them being ions. The operators $\mathcal{T}$ and $\mathcal{C}_0$, computed by CAST3M and CHESS, respectively, are defined by:

$$\mathcal{T}(\phi_t, \phi_m, C_i) = \nabla\cdot(\mathbf{D}^*(\phi_t, \phi_m)\nabla(C_i)) \quad (3)$$

$$\mathcal{C}_{0i}(C_i) = \begin{cases} \text{precipitation}: \quad K_m^p = \prod_{i=1}^{N} [e_m]\left[e_i^{z+}\right]^{-\nu_{im}} \\ \text{dissolution}: \quad K_m^d = \prod_{i=1}^{N} \left(\left[e_{ia}^{z+}\right][e_m]\right)^{-1}\left[e_i^{z+}\right]^{\nu_{im}} \end{cases} \quad (4)$$

where K_m^d and K_m^p are the equilibrium constants of the dissolution or precipitation reactions, V_{im} designates the stoichiometric coefficients, e_m denotes a mineral species, e_{ia}^{z+} an ionic species consumed in the dissolution reaction and e_i^{z+} an aqueous species that forms in the interstitial solution, z being an integer. The square brackets surrounding given species designate its activity, which is computed by means of the modified Davies method in our simulations. $\mathbf{D}^*$ is the second-order diffusivity tensor which is assumed to only depend on the current microstructure of the material, i.e. it is constant for all ionic species. This constitutes an important simplifying hypothesis, similar to the one adopted for instance in the HYTEC chemo-transport code [30]. Moreover, the dispersion is neglected and no overall movement of water is considered in our simulations (water pressure is assumed homogeneous throughout the sample), so that the ionic migration only results from molecular diffusion. Finally, we may reasonably consider that the material is locally isotropic, which means that $\mathbf{D}^* = D^*\mathbf{I}$, with D^* the diffusion coefficient and $\mathbf{I}$ the second-order identity tensor.

The multi-species reactive transport problem described in Eqs. (2)–(4) is solved by means of a sequential iterative algorithm [31], each chemical–transport loop being evaluated in two steps. The first one consists in computing with CAST3M the transport of aqueous species due to concentration gradients by means of the finite volume method. The medium is thus represented by subvolumes V_I constituted by the elements of the mesh, each comprising mineral phases and N aqueous species. A fixed point algorithm implicit in time is used to solve the transport equations [32]. In the second step, the mineral composition is updated to conform with the newly calculated ion concentrations by means of the chemical code CHESS. Both porosity and diffusivity are then re-evaluated from this updated mineral composition. The diffusion coefficient is estimated by a homogenization model which takes into account independently the capillary porosity and the one of the gel pores included in the C–S–H phase [33,34].

3.3.2. Practical considerations

To simplify the simulations, the following hypotheses were adopted. We considered that the migration of all ionic species took place perpendicularly to the surface exposed to the ingress, so that the degradation was one-dimensional, i.e. the mineralogy was exactly the same everywhere in a plane parallel to the surface. Accordingly, a simple mesh composed of one row of 200 elements was used in the computations and represented half of the sample thickness, i.e. 5 mm. Moreover, to simulate the experiments as realistically as possible, we had also modelled the volume containing the Na_2SO_4 solution in order to reproduce the periodic solution changes. Then, the profiles of ion concentrations in the solution were calculated as in the specimen, which led to a precise evaluation of the boundary conditions at the specimen surface. This volume containing the Na_2SO_4 solution consisted in additional elements whose phase properties were set to classical values for water (i.e. porosity equal to 1 and diffusion

coefficient equal to 2×10^{-9} m^2/s). The dimension of the mesh of volume containing the Na_2SO_4 solution perpendicular to the attacked surface was estimated as follows: the total exposed surface of the specimen was assumed to result from all lateral surfaces of the prisms except the ones at the edges (where the sensors for dimension measurements were located), i.e. $2\times(1+4)\times16=160$ cm^2. Given the experimental liquid/solid volume ratio of 4 to 1, and since the volume of the specimen was 64 cm^3, the ratio of the volume containing the Na_2SO_4 solution over specimen surface was $4\times64/160=1.60$ cm. This length corresponded then to the sought dimension of the batch perpendicular to the specimen surface, and was modelled numerically by 50 elements. The simulated concentrations of chemical species in the volume containing the Na_2SO_4 solution evolved appreciably between two solution changes, leading to significant variations of boundary conditions at the specimen surface. The time steps were not imposed specifically and were corrected by the code so as to obtain the number of iterations prescribed by the user for achieving the convergence at a given precision. Typically the time step was on average 50–100 s for the case with 44 g/L Na_2SO_4 and 100–200 s for 4 g/L Na_2SO_4, for a convergence in 10 iterations with a relative precision of 0.01%. The corresponding total computation time was about 1 day and 4–5 days, respectively, without parallelization. The latter aspect will be available soon and will considerably reduce the computation cost.

The C–S–H phase was modelled as a composite of jennite ($C_{1.7}SH_{2.1}$), tobermorite ($C_{0.8}SH_{1.3}$) and SiO_2; for the reactive transport modelling these three basic minerals were considered as three separate solids, as solid solution models are not yet available in ALLIANCES.

4. Sulfate ingress results

4.1. Composition of the hydrated cement before sulfate interaction

Before exposure to sulfate solutions, mortars as well as cement paste sample were hydrated in saturated lime solutions for 28 days. The XRD and TGA data given in [3,35] of the paste samples showed that, after 28 days, besides some unhydrated clinker, mainly portlandite, C–S–H, ettringite as well as monosulfate was present. The EDS analysis of the mortar samples showed the same phase assemblage [35]. Thermodynamic modelling of the hydration of the cement as a function of time indicates that after 28 days besides C–S–H, portlandite, monosulfate, ettringite, some hemicarbonate and hydrotalcite are present (Fig. 1), which agrees well with the experimental observations for this cement as reported in [3,35].

4.2. Experimental observations

The mass gain and expansion results have been discussed in detail in a previous paper [3] and are summarised below to ease comparison between experimental and modelling results. The mortar samples of the cement showed a higher expansion and mass gain in the presence of 44 g/l Na_2SO_4 concentrations than at 4 g/l, or in the presence of saturated lime solutions (Fig. 2).

The analysis of the solid phase assemblage by SEM/EDS as given in [3,35] indicated in the unaffected core regions of the sample the presence of portlandite, C–S–H, ettringite and monosulfate. Nearer to the surface, no monosulfate was detected in the samples exposed to Na_2SO_4 solutions but a higher fraction of ettringite (as indicated by the bars given at the bottom of Fig. 3). In the outermost layer (0–1 mm) beside C–S–H only ettringite could be detected in samples exposed to 4 g/l Na_2SO_4 solutions. The EDS analysis [35] indicated also a decrease of the Ca/Si ratio of the C–S–H from the core to the outermost layer. Gypsum was found in the samples exposed to 44 g/l Na_2SO_4 [3,35]. Gypsum, however, was found to have little effect on the observed expansion but to form rather in already existing pores resulting in no or very limited additional expansion [3].

The ingress of sulfate into the mortar samples as well as the leaching of Ca had been followed by SEM/EDS. Already after 8 weeks of exposure time clear differences in the SO_3 profiles could be observed (Fig. 3). Both the samples immersed in 4 and in 44 g/L of Na_2SO_4, showed a clear increase of SO_3 near the sample surface, while the changes in CaO were still small. With time the SO_3 front progressed further into the sample with a maximal SO_3 content around 20 wt.% and 10 wt.% for 44 and 4 g/L of Na_2SO_4, respectively (Fig. 3, [35]). Similarly, measured CaO was lowered with time and the depression progressed further into the sample. The content of CaO decreased from approximately 60 wt.% before exposure to 45 wt.% after 9 months in the samples exposed to 4 g/l Na_2SO_4.

The changes associated with Na_2SO_4 ingress as reported in [3,35] are consistent with other data reported in the literature: an inward movement of the reaction front with time, destabilisation of portlandite and AFm phases, decalcification of the C–S–H, formation of ettringite and in the presence of higher Na_2SO_4 concentrations, the precipitation of gypsum [1,2,36–38]. For samples exposed for years to

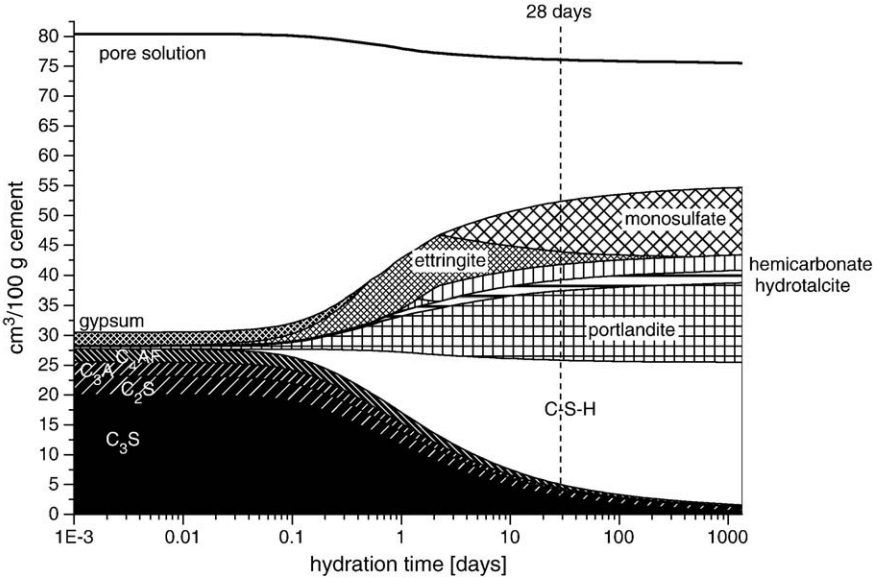

Fig. 1. Modelled phases changes during the hydration of the OPC. Volume expressed as cm^3/100 g unhydrated cement.

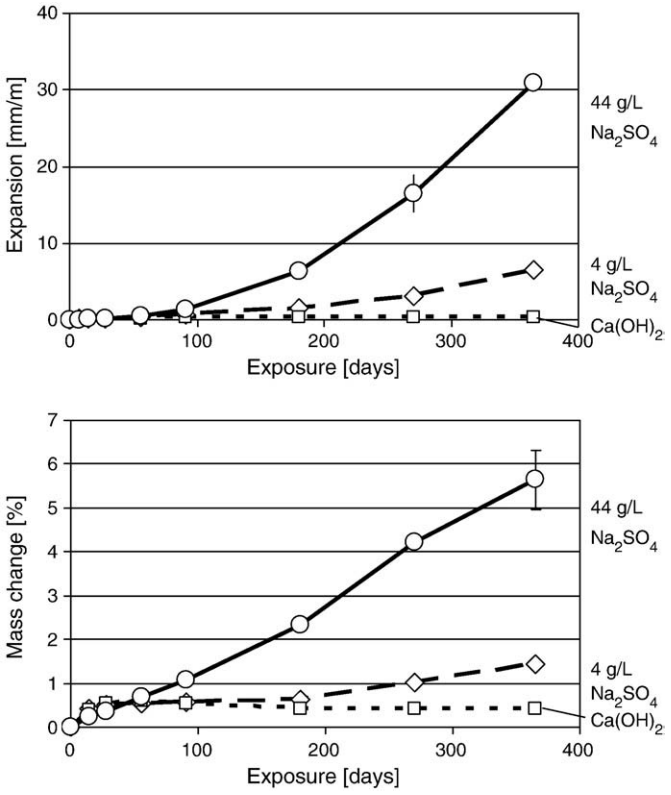

Fig. 2. Expansion and mass change of mortar samples immersed in 44 and 4 g/L Na_2SO_4 solutions. Reference samples were immersed in saturated $Ca(OH)_2$ solutions. Experimental data from [3].

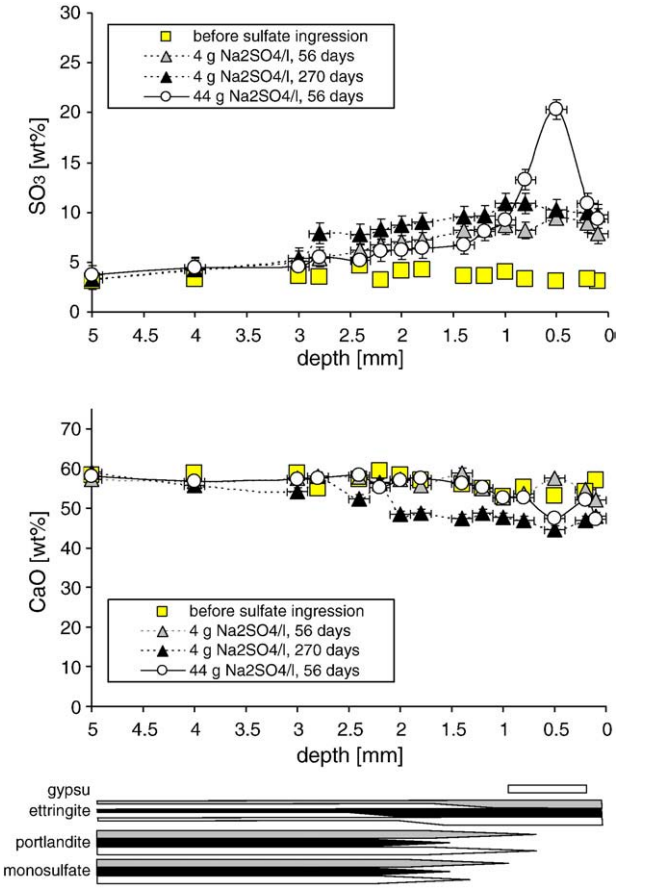

Fig. 3. Measured sulfate and calcium distribution in mortar samples before sulfate ingress and in samples immersed in solutions containing 44 g/L Na_2SO_4 or 4 g/L Na_2SO_4 as determined by SEM/EDS. The presence of solid phases as determined by EDS is indicated by bars at the bottom of the figure. The thickness of the bars indicate the relative amount of solids observed. Experimental data from [3,36].

high sulfate solutions, also the formation of thaumasite has been reported [3,36].

4.3. "Pure" thermodynamic modelling of sulfate ingress

The phase assemblage was calculated as a function of the ratio of Na_2SO_4 solution to the volume of the hydrated cement. The core of the sample is not or hardly affected by the presence of Na_2SO_4, while the outermost layer is in contact with a large amount of Na_2SO_4 solution. In the calculations given in Figs. 4–7, the unaffected core is represented at left hand of the Figs. 4–7 by 10^{-3} mL Na_2SO_4 solution added/cm^3 mortar, while the results obtained by equilibrating the mortars mathematically with larger amounts of Na_2SO_4 solution mimic the changes associated with sulfate ingress. As mentioned before this approach has the advantage that the calculations are very fast and flexible but the disadvantage that the calculated data relate neither to time nor to distance and merely the sequence of changes is reproduced. The approach also implies that sodium and sulfate ingress always at the same rate.

4.3.1. Solid phase assemblage

Thermodynamic modelling predicted in the hydrated core of the mortar sample exposed to 4 g/L Na_2SO_4 the presence of C–S–H, portlandite, monosulfate, ettringite and smaller quantities hydrotalcite and hemicarbonate (Fig. 4A). The presence of C–S–H, portlandite, monosulfate, and ettringite agrees with the experimental observations. Upon ingress of Na_2SO_4 solution, the AFm phases and a part of the portlandite were calculated to convert to ettringite until all aluminium (and iron) available was present as ettringite. Closer to the sample surface, the remaining portlandite and the C–S–H were leached. The sequence as calculated by "pure" thermodynamic modelling agreed with the sequence observed in different experimental studies (see Fig. 3 and [1–3,36]).

The sample immersed in 44 g/L Na_2SO_4 showed the same sequence (Fig. 4B). However, relatively less solution was needed for the transformation of AFm and portlandite into ettringite. At the higher sulfate concentration gypsum formation was predicted which agreed again with the experimental observations for the high Na_2SO_4 concentration (Fig. 3a).

4.3.1.1. Porosity. Based on the calculated volume of the solids, the total and capillary porosity were derived (Fig. 5). The calculated (total) porosity of the system decreased from the core of the sample towards its surface as ettringite precipitated, which filled up the available pore space. Higher Na_2SO_4 concentration and the associated precipitation of gypsum reduced the available pore space further to approx. 5% at the place where the maximal amount of gypsum was precipitated. The calculated total porosity included also the gel pores associated with C–S–H. The capillary porosity, i.e. total − gel porosity, decreased from 12 to less than 1 vol.% and increased near the surface of the system. The calculated capillary porosity showed a similar behaviour as the total porosity (Fig. 5). In the case of the interactions with the 44 g/L Na_2SO_4 solution, a reduction of the capillary porosity to approximately zero was calculated.

The total volume of the solids exceeded neither in the presence of 4 or 44 g/l Na_2SO_4 the initial volume of the paste (82 cm^3/100 g of cement, including water) indicating that theoretically no expansion should have taken place, if the solids had precipitate in the empty pore space only. Various different theories have been put forward to explain the mechanism of sulfate expansion. Recent theories support the idea that the crystallisation pressure due to the precipitation of ettringite from oversaturated solutions develops in small pores

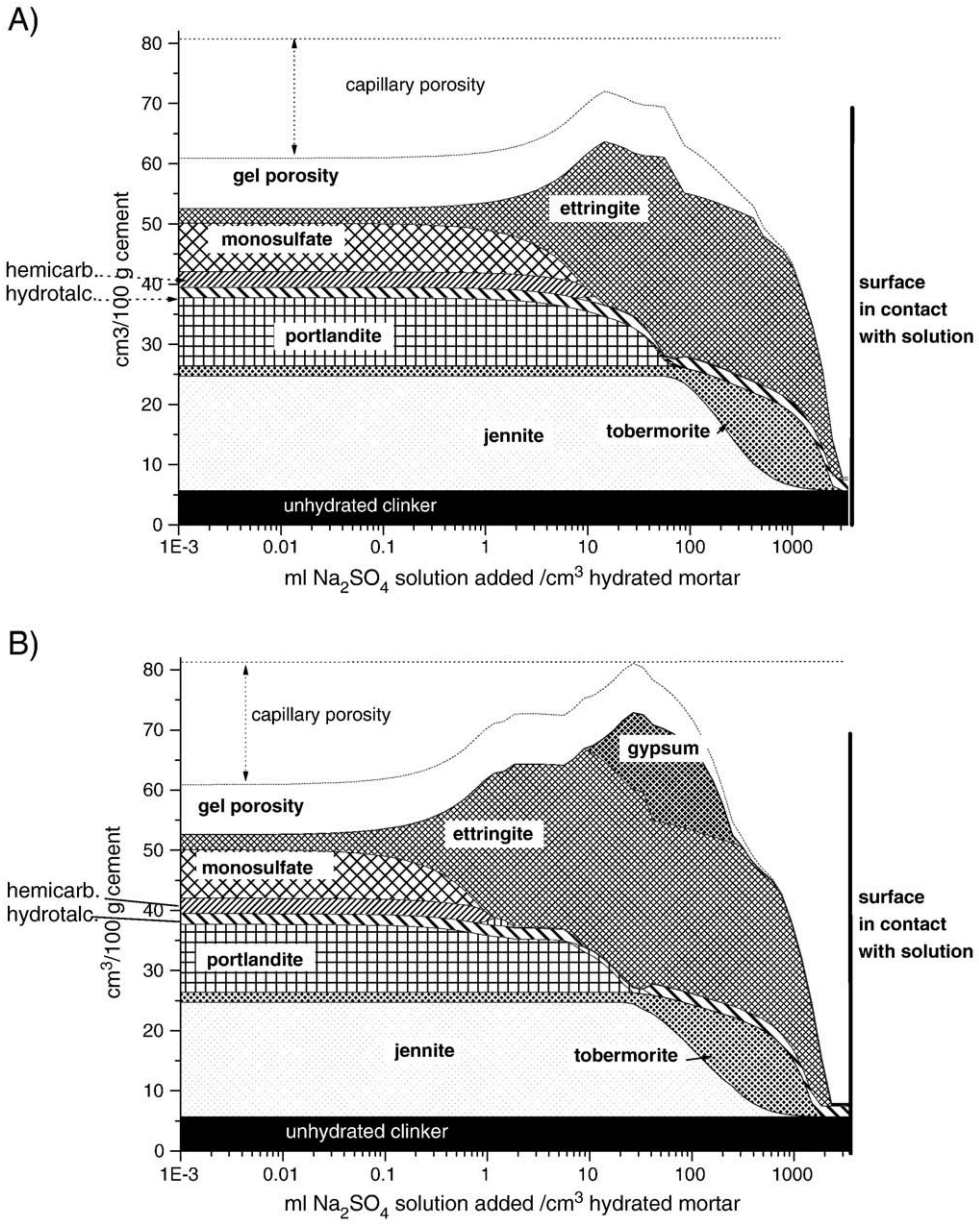

Fig. 4. Phase assemblage of the mortar samples immersed in A) 4 g/L Na_2SO_4 and B) 44 g/L Na_2SO_4 as calculated with GEMS.

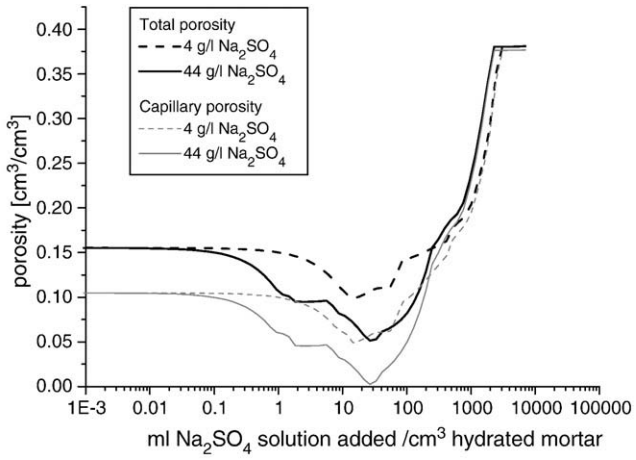

Fig. 5. Total and capillary porosity of the mortar samples immersed in 4 g/L Na_2SO_4 and 44 g/L Na_2SO_4 as calculated with GEMS.

(typically<0.1 μm) in the hydrated cement matrix, resulting in stress and subsequent expansion of the matrix, as suggested by Scherer [39]. The formation of ettringite in the matrix and only partially in empty large pores has been observed experimentally by the formation of ettringite within the C–S–H while empty air voids and large pores were visible in the same region of the sample (e.g. [3]).

4.3.2. Calculated SO_3 and CaO profiles

Thermodynamic modelling allows the calculation of SO_3 and CaO profiles which are presented in Fig. 6 as a weight fraction of the mass of the unhydrated cements. The calculated weight fractions of SO_3 and CaO are shown (i) as calculated, not considering the changes in mass due to the formation of gypsum, ettringite and due to leaching. This relates the calculated SO_3 and CaO profiles to 100 g of the original cement and reproduces the changes of solid phase as e.g. visible in the grey scale of SEM pictures. The calculated weight fractions of SO_3 and CaO according to (i) are represented by the black lines in Fig. 6 and illustrate the accumulation of sulfate as the sodium sulfate solutions ingressed into the mortar. Similarly, the leaching of calcium near the

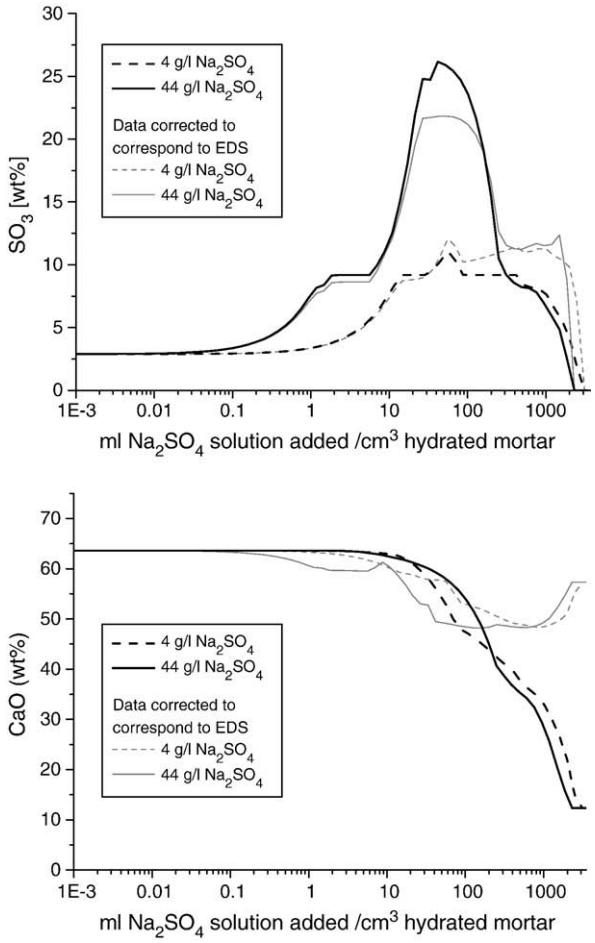

Fig. 6. SO_3 and CaO profile of the mortar samples immersed in 4 g/L Na_2SO_4 and 44 g/L Na_2SO_4 as calculated with GEMS.

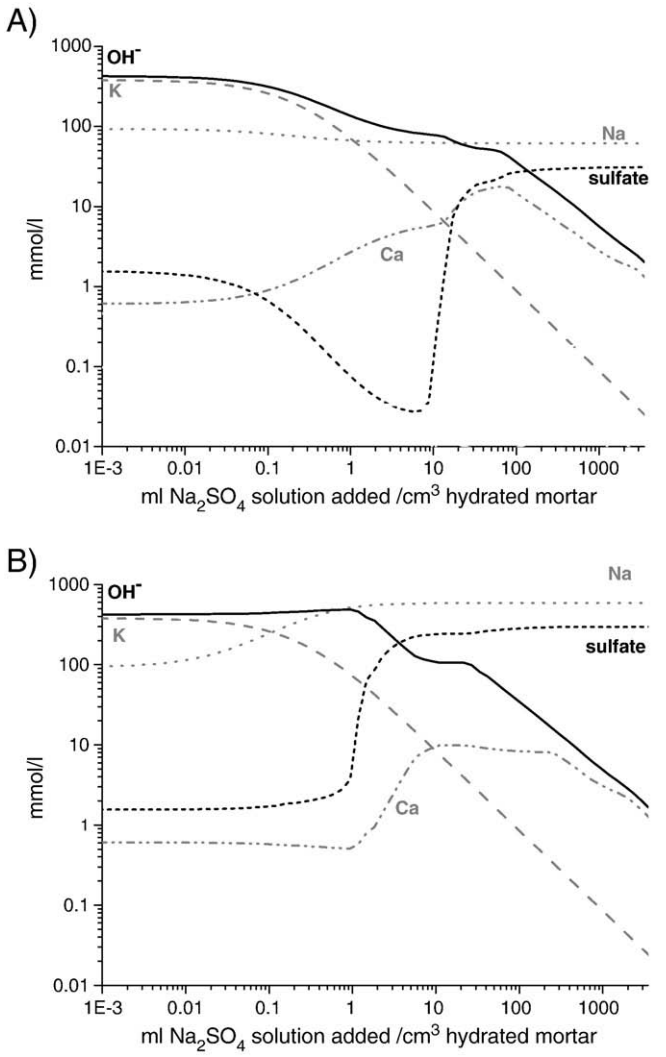

Fig. 7. Concentration in the mortar samples immersed in A) 4 g/L Na_2SO_4 and B) 44 g/L Na_2SO_4 as calculated with GEMS.

sample surface is visible. In the core of the sample the calculated and the measured SO_3 fractions correspond to the total SO_3 present in the cement while they increase nearer to the surface where the cement interacted with the ingressing Na_2SO_4 solution increased towards to surface; the increase depends on the concentration of the Na_2SO_4 solution (Fig. 6).

The calculated CaO profile shows a strong leaching near the surface of the sample which agrees with the lowering of Ca/Si ratio near the surface observed experimentally [35]. The concentration of the Na_2SO_4 solution seemed to have a minor effect as the leaching was mainly due to the quantity of water in contact with the solids. In the presence of higher Na_2SO_4 concentrations a slightly stronger leaching of the cement was calculated as the solubility of the ettringite increases with increasing ionic strength.

In addition, the calculated weight fractions of SO_3 and CaO are shown (ii) also as a weight fraction of the mass of cement present (without water, grey lines in Fig. 6) which relates directly to the EDS measurements. Comparison of these data with the measured data as given in Fig. 3 showed qualitatively the same changes during the ingress of sulfate and the calculated weight fractions agreed with the measured weight fractions as given Fig. 3. Near the surface of the sample the total amount of solids decreased strongly due to leaching, thus the calculated CaO profiles remained constant or increased slightly, when they were normalised to the amount of solid cement still present (i.e. grey lines in Fig. 6). At the outermost layer, where nearly all of the cement was calculated to be leached, the calculated wt.% corresponded to the small quantities of clinker assumed still to be present.

4.3.3. Concentrations in the pore solution

Simultaneously to the hydrate assemblage calculation, the composition of the liquid phase within the mortar was determined. The calculated composition of the pore solutions, equivalent to the unaffected part of the samples, indicated high concentrations of potassium and sodium hydroxide (Fig. 7). In addition, lower concentrations of approx. 1 mmol/l were calculated for sulfate, calcium and aluminium, which correspond to the concentrations measured in hydrated CO_2-poor cements [27,40].

Near the surface of the solid specimen a significant influence of the concentrations used in the reacting Na_2SO_4 solutions was calculated. In the case of 4 g/l Na_2SO_4, the calculated sodium concentrations decreased slightly while the sulfate concentrations increased near the surface of the sample. In the case of higher concentrations of sodium sulfate, both the sodium and sulfate concentrations in the pore solutions were calculated to increase towards the surface (Fig. 7). The sodium present in the reacting solution ingressed farther into the mortar samples than the sulfate, as the major fraction of the ingressing sulfate precipitated as gypsum and ettringite (Fig. 4). This separation of the reacting solution influenced the calculated hydroxide concentrations strongly. While in the core of the mortar sample the hydroxide concentration was determined by the amount of alkalis present in the cement, they increased slightly due to the ingressing Na before they decreased again (Fig. 7B). In the presence of

4 g/L Na_2SO_4 a continuous decrease of the hydroxide concentration from approx. 400 mmol/L (pH 13.8) in the core of the solid sample to less than 1 mmol/L (pH<12) near the surface was calculated. These changes in pH were also mirrored in the calculated Ca concentrations. In solutions which were equilibrated with portlandite, increasing pH values resulted in lower Ca concentrations and vice versa. Thus, the thermodynamic calculations illustrated that the concentrations in the reacting Na_2SO_4 solutions did not only influence sodium and sulfate but also the concentrations of the other elements present in the pore solutions.

4.4. Chemical–transport modelling

In this section the results of the numerical simulations carried out with ALLIANCES are presented. All chemical reactions were assumed to be at equilibrium and the same diffusion coefficient was applied to all aqueous species.

4.4.1. Mineralogical profiles

The mineralogical profiles in terms of solid concentrations in the mortar obtained with ALLIANCES at 56 days of exposure are depicted on Fig. 8 as a function of the depth from the surface exposed to the sulfate solution for the cases of 4 g/L Na_2SO_4 (A) and 44 g/L (B) of sodium sulfate. These results are also shown on Fig. 9 in the same representation and with the same units (cm^3/100 g of cement) as in Fig. 4 to ease comparison.

From these results, we observe that portlandite was totally dissolved up to 0.5 mm from the surface in both cases of sulfate solution. In contrast, the degradation depth, as characterized by the distance at which monosulfate has disappeared, was 2.8 and 1.3 mm for 44 g/L and 4 g/L Na_2SO_4, respectively. The degradation was then much more pronounced in the former case, due to the higher sulfate concentration which increased the concentration gradients and consequently its diffusion within the material. Accordingly, less of the higher concentrated solution was needed to transform all AFm into ettringite, resulting in a faster apparent diffusion. However, such a much faster ingress at higher concentrations was not visible in the experimental results as given in Fig. 3, where a comparable degradation depth was observed. This disagreement could be explained by an imprecise estimation of the diffusivity, in particular in the degraded zone of the material which was subjected to important variations of the phase assemblage. Indeed, the model predicting the diffusivity as a function of the mineral volume fractions and defined in [33,34] has not been validated (i.e. confronted to experimental data) for intermediate degraded states of the material.

Another significant distinction between the two cases concerns the phase assemblage near the surface. The simulations predicted the precipitation of gypsum between about 0.2 and 0.5 mm in the 44 g/L

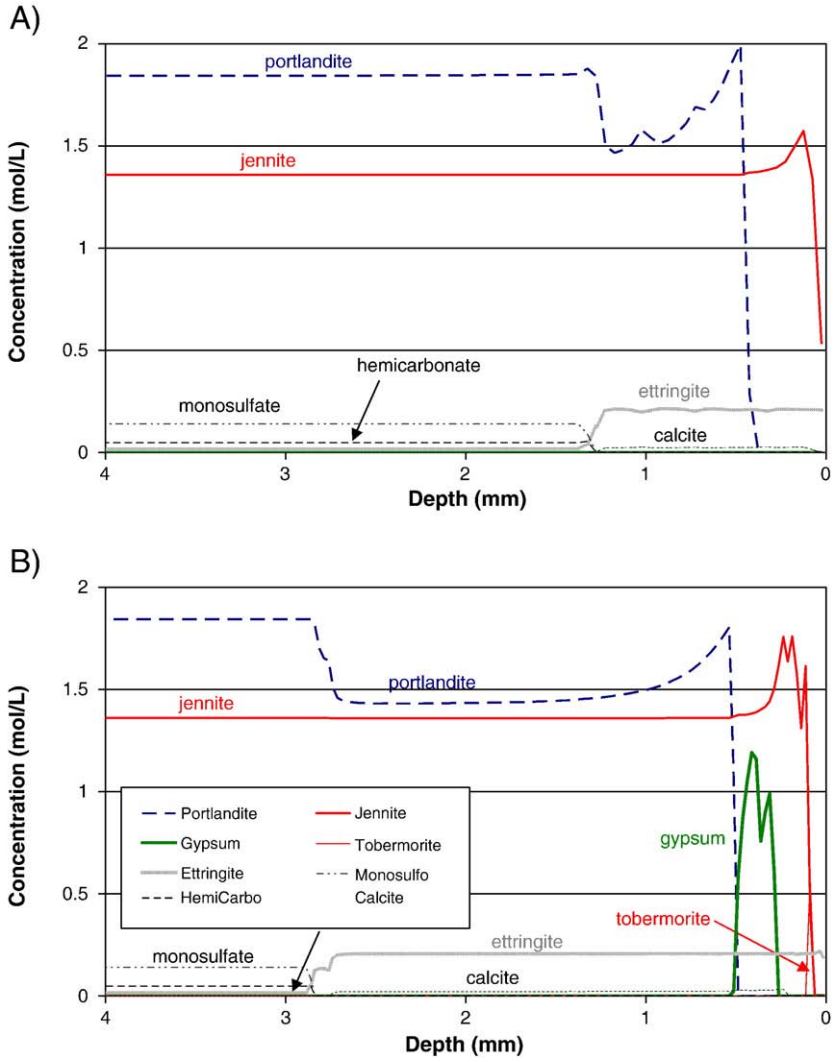

Fig. 8. Simulated mineralogical profiles of the mortar samples immersed in A) 4 g/L Na_2SO_4 and B) 44 g/L Na_2SO_4 as obtained with ALLIANCES at 56 days.

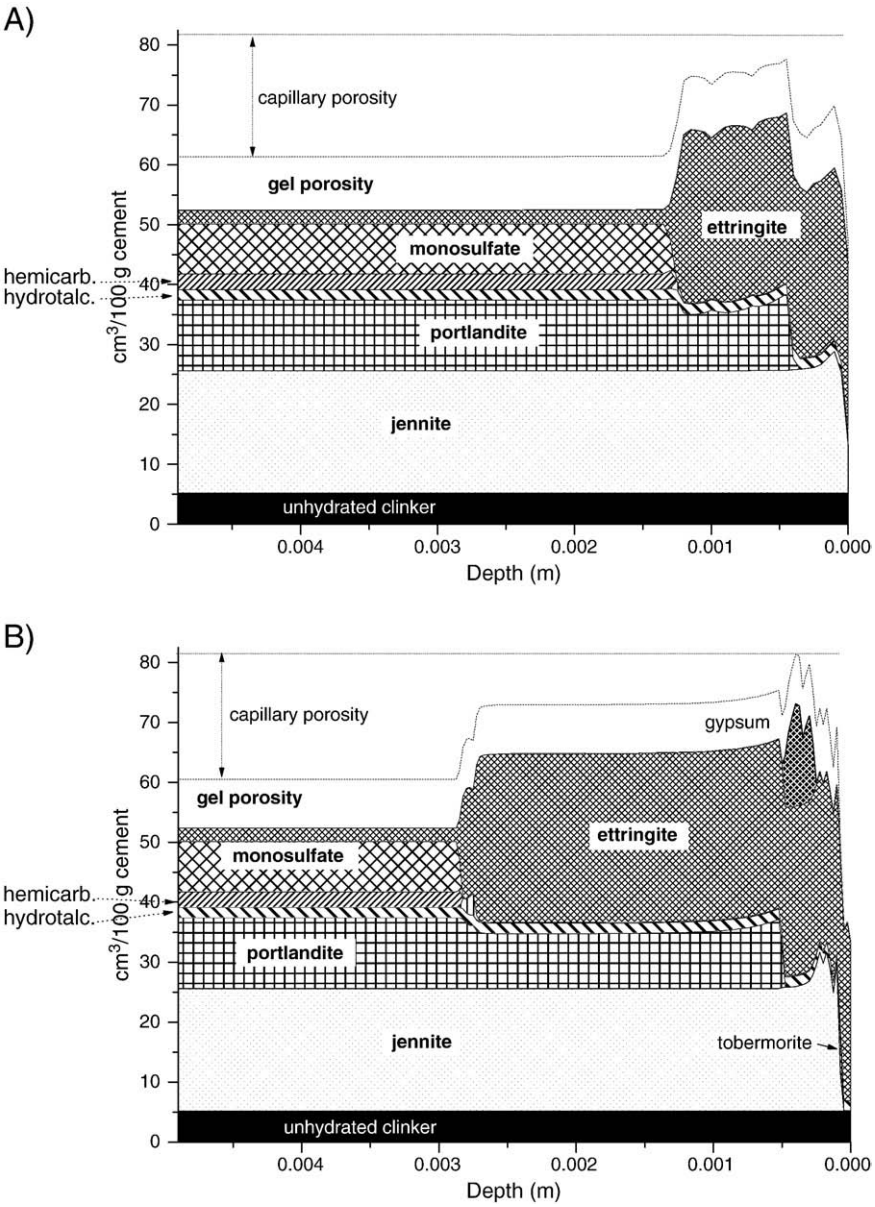

Fig. 9. Simulated mineralogical profiles of the mortar samples immersed in A) 4 g/L Na_2SO_4 and B) 44 g/L Na_2SO_4 as obtained with ALLIANCES at 56 days.

Na_2SO_4 case, while no presence of this phase was calculated in the 4 g/L Na_2SO_4 case. Moreover, jennite decomposed into tobermorite in a very narrow region close to the surface in the former case, whereas no tobermorite precipitated in the latter one, which seems to indicate a more intense degradation when the specimen was in contact with a more aggressive sodium sulfate solution. No SiO_2 precipitation was predicted, even in the 44 g/L Na_2SO_4 case in which tobermorite was totally dissolved in the outermost layer.

Similarly to Subsection 4.3.1, the capillary and gel porosity profiles were calculated in both 4 and 44 g/L sodium sulfate cases at 56 days. The results are shown on Fig. 9 and are consistent with the ones displayed on Fig. 5, i.e. the capillary porosity is reduced in the degraded regions where ettringite was formed, and is almost completely filled in the zone where gypsum further precipitated.

In order to investigate the effects of the periodic solution changes on the hydrate assemblage, a further simulation was carried out in the 4 g/L Na_2SO_4 case in which a continuous exchange of the Na_2SO_4 solution was considered. This was achieved by assuming that the concentrations at the specimen surface remained constantly equal to the ones of the initial sulfate solution. Fig. 10 presents the results at 270 days when only periodic changes were taken into account A) and when a continuous exchange was assumed B). We observe that the degradation was more intense and slightly deeper in the case B) (continuous exchange) than in the case A), periodic exchange. Indeed, the depth at which AFm was transformed into AFt was 2.5 mm and 2.2 mm and portlandite was totally dissolved at 1.6 mm and 0.7 mm for the cases B) and A), respectively. We also remark in the case B) the presence of tobermorite (which replaced jennite) in a zone of about 1 mm large, and the complete dissolution of ettringite and tobermorite from the surface to 0.3 mm depth, indicating a more severe degradation. If the solution would not have been exchanged at all, we calculate a strong decrease of sodium and sulfate concentrations, which is consistent with experimental observations [41], and less degradation than the case of periodic exchange A) or continuous exchange B). From this comparative analysis, we may conclude that the periodic changes and the corresponding evolution of the concentrations in the ingressing solution should be considered in the simulations for better representing the experiments, as they lead to significantly different results than in the case where the composition of the solution is kept unchanged.

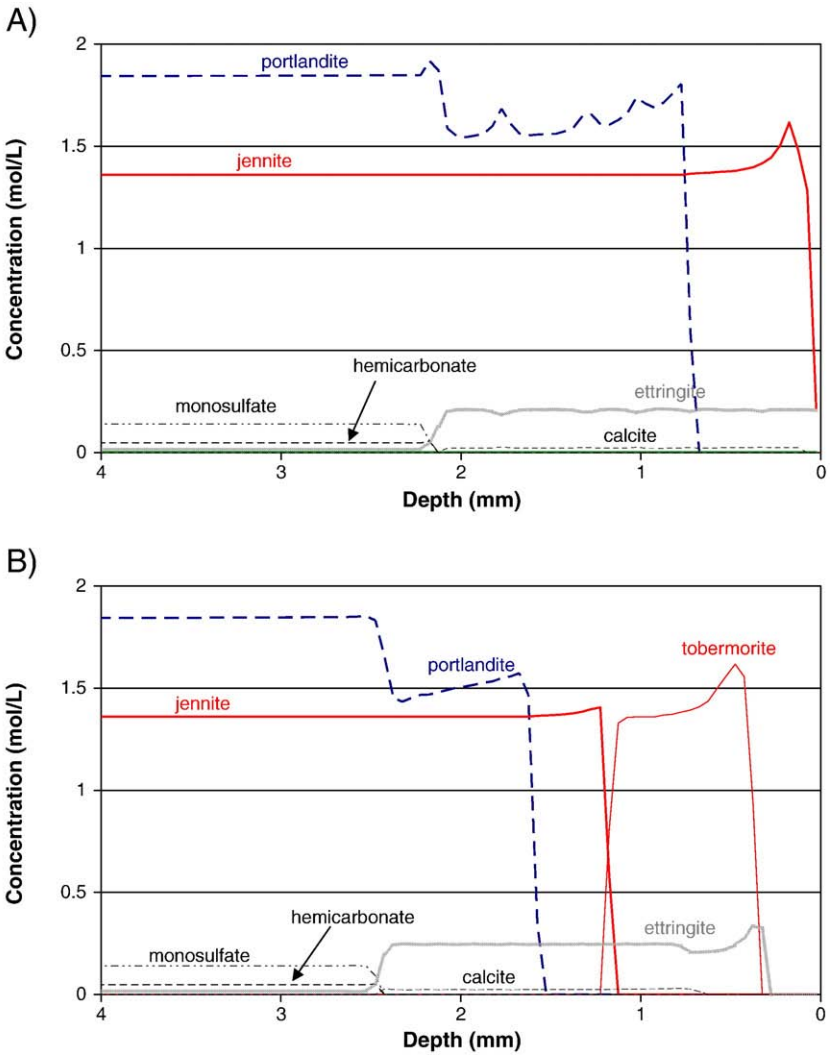

Fig. 10. Simulated mineralogical profiles of the mortar samples immersed in 4 g/L Na_2SO_4 A) with solution changes and B) in a solution with constant boundary conditions (continuous exchange of solution) as obtained with ALLIANCES at 270 days.

The small peaks observed on portlandite and ettringite concentration in the Fig. 10A) did not result from the numerical algorithms and possible oscillations. They are attributed to the evolving boundary conditions at the specimen surface and more precisely to their abrupt variations when the Na_2SO_4 solutions were changed. This point is supported by the fact that such peaks were not present in the case B) where the boundary conditions were constant. These non-smooth mineral profiles are also visible - though to a lesser extent - for gypsum in the 44 g/L Na_2SO_4 case (Fig. 8 and Fig. 9).

As a last remark, we may emphasize that the concentration profiles of most minerals exhibited a peak before their dissolution. This was more particularly visible for portlandite and jennite, especially in the 44 g/L Na_2SO_4 case. One explanation could be that a part of the released ions could migrate towards the core of the specimen due to diffusion (another part migrating towards the exterior and the rest being involved locally in chemical reactions) when dissolution occurred. The released ions then re-precipitated behind the dissolution front. This argument is suggested by the fact that in the simple thermodynamic modelling (Fig. 4), where no "back-diffusion" can be considered, no such peaks were observed at the dissolution front. To our best knowledge, such feature seems not to have been reported experimentally in the literature, indicating that it could be due to one of the modelling assumption (as for instance the absence of kinetics aspects in the chemical reactions), or to the numerical methods employed for solving the problem.

4.4.2. Calculated SO_3 and CaO profiles

The simulated profiles of weight fractions of SO_3 and CaO are depicted in Fig. 11. Again, two representations are plotted to ease comparison with the pure thermodynamic modelling (Fig. 6 and Subsection 4.3.2) and with the experimental data of Fig. 3, also reported on Fig. 11. The first representation does not consider the changes in mass due to the precipitation and dissolution of hydrates and relates to the initial mass of cement (black lines Fig. 11). The second representation takes into account these mass changes (grey lines Fig. 11), and can be directly compared to the EDS analyses.

The simulations related to the initial mass of cement show clearly the regions where sulfate accumulated. The calculated SO_3 increased near the surface where ettringite precipitated. For the higher Na_2SO_4 concentration solution, the zone where gypsum precipitated is also clearly visible with values of weight fraction of SO_3 reaching nearly 30%. This is, together with a greater degradation depth, an essential difference with the 4 g/L Na_2SO_4 case. The simulated CaO profiles exhibit a significant decrease in the vicinity of the surface, indicating an intense leaching of the material. This aspect is slightly more

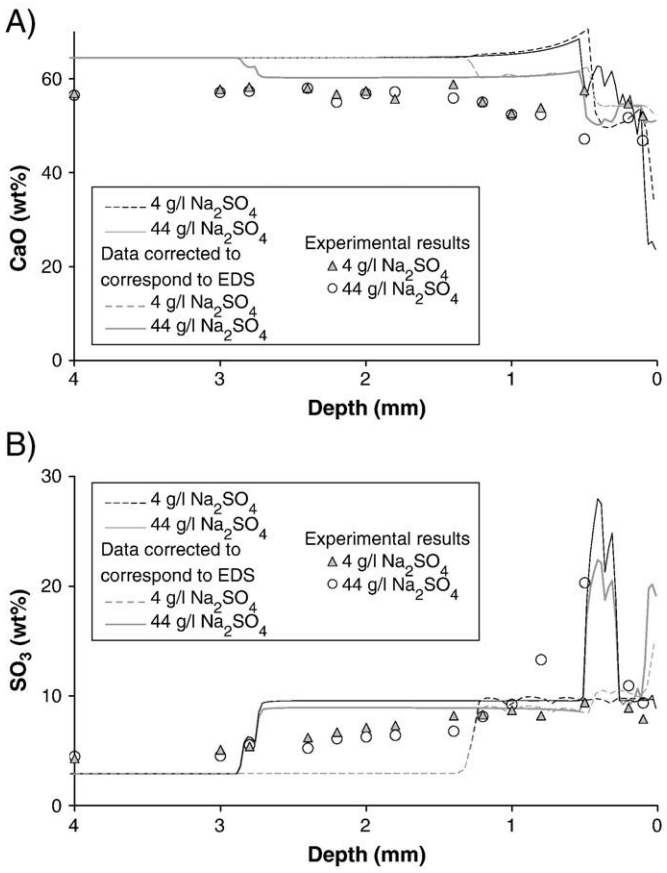

Fig. 11. Numerical CaO A) and SO_3 B) profiles of the mortar samples immersed in 4 g/l Na_2SO_4 and 44 g/l Na_2SO_4 as obtained with ALLIANCES at 56 days. Experimental results of Fig. 3 are also reported (symbols).

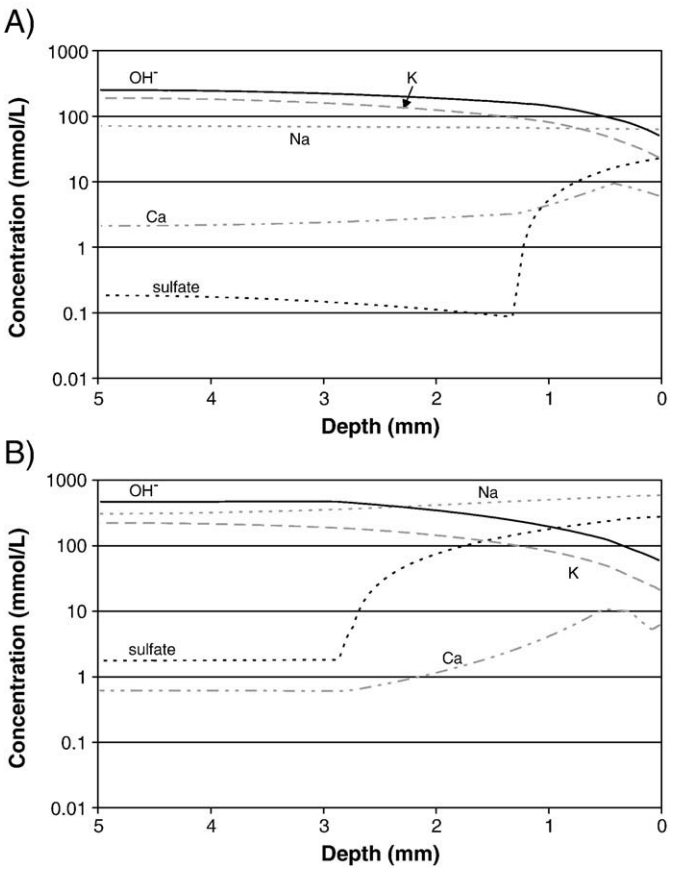

Fig. 12. Numerical concentration in the mortar samples immersed in A) 4 g/l Na_2SO_4 and B) 44 g/l Na_2SO_4 as obtained with ALLIANCES at 56 days.

pronounced in the case of the higher Na_2SO_4 concentration, where the depletion of portlandite due to leaching is noticeable.

The second type of calculation relates the SO_3 and CaO quantities to the total mass of solid present locally. The main differences between these results and the preceding ones are in the degraded regions, since in these zones both precipitation and dissolution of minerals had occurred. Although not totally satisfactorily, the SO_3 profiles obtained are quantitatively quite close to the experimental data, with a magnitude of about 22% in the gypsum precipitation zone for the higher Na_2SO_4 solution. However the zone where gypsum precipitated is narrower in the simulations than in the experiments. Moreover, the numerical dissolution and precipitation fronts of portlandite, gypsum and ettringite are very abrupt, whereas these changes happened more progressively in the experiments. Also, as already mentioned in the previous subsection, the numerical results show a significant difference between the two sulfate solutions (i.e. a much larger degradation depth in the 44 g/L Na_2SO_4 case), which was not observed experimentally. Instead, the EDS results exhibited comparable profiles, except in the zone where gypsum precipitated. Finally, in the outermost layer, the calculated SO_3 profile shows a significant increase due to the complete leaching of the C–S–H phase, which was not observed in the experimental data. The CaO profiles (grey lines in Fig. 11 A) are also considerably affected, in particular in the vicinity of the surface.

4.4.3. Concentrations in the pore solution

The simulated pore solution composition in the mortar samples is presented at 56 days in Fig. 12 for the two sulfate solutions. We observe that the two regions constituted by non-degraded and degraded parts of the samples (i.e. behind the degradation front and from this front to the specimen surface, respectively) are clearly visible in the calculated concentrations. The non-degraded zone exhibits low concentration variations while the degraded zone displays important changes, in particular for sulfate ions. This is due to the reaction of these sulfate ions migrating from the Na_2SO_4 solution and leading to precipitation of ettringite.

Potassium ions present initially in the material at high concentration diffused towards the Na_2SO_4 solution, which was free from this species after each change. Likewise, OH^- concentration decreased from about 430 mmol/L (pH = 13.51) to 250 mmol/L (pH = 13.28) for 4 g/l sodium sulfate solution. However, for 44 g/L Na_2SO_4, OH^- concentration in the centre of the specimen slightly increased up to 470 mmol/L (pH = 13.54), due to the penetration of sodium from the higher concentration in the Na_2SO_4 solution and the fact that the sulfate reacted almost entirely to form ettringite.

These significant changes of alkalis and hydroxide concentrations with high initial concentrations led also to important variations of calcium and sulfate in the non-degraded zone of the samples. Indeed, there was a difference of about one order of magnitude in calcium and sulfate concentrations between the two cases. Note that the calcium concentration near the samples surface was not 0 but reached about 6 mmol/L at 56 days (see the next subsection).

4.4.4. Changes in the ingressing Na_2SO_4 solutions

Not only the concentrations within the specimen changed but also the composition of the ingressing Na_2SO_4 solutions varied drastically during the tests. Fig. 13 presents the numerical profiles of A) sulfate, B) calcium and C) sodium concentrations in the ingressing solution as a function of time, for the points located at 0.5, 4.0, 8.0 and 15.8 mm from the specimen surface, and in the 44 g/L Na_2SO_4 case. The solution changes at 7, 14 and 28 days appear clearly on the curves as they led

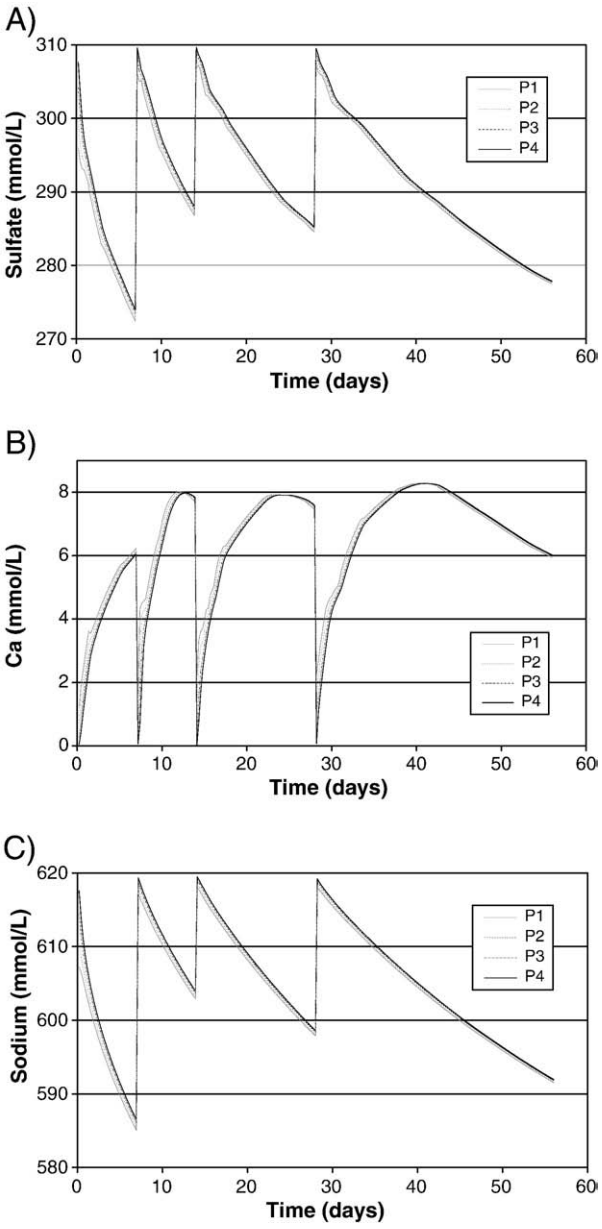

Fig. 13. Time evolution of the concentration of A) sulfate, B) calcium and C) sodium in the solution for the 44 g/l Na_2SO_4 case as obtained with ALLIANCES, for the points P1, P2, P3 and P4 located at 0.5, 4.0, 8.0 and 15.8 mm from the specimen surface.

to instantaneous variations of concentrations. We observe that, except in the first 1–2 days following the solution changes, the concentrations at the four considered points were very close. The calculated sulfate concentration decreased in the Na_2SO_4 solution from about 310 to a value of 273 mmol/L at 7 days just before the solution was changed. At 56 days this concentration was near 278 mmol/L. Such a decrease of the sulfate concentration in the ingressing Na_2SO_4 solution with interaction time is consistent with experimental results [41]. On the other hand, the calcium concentration was calculated to increase from 0 to a little more than 6 mmol/L at 7 days, and was also equal to 6 mmol/L at 56 days. However, it is interesting to notice that, except for the first exposure period, the calcium concentration systematically reached a maximum value of about 8 mmol/L before slowly decreasing. This indicates that after each solution change calcium was first leached from the specimen, then in a second stage it re-entered within the material. This result corroborates the conclusions drawn when analysing the Fig. 10A) and B), i.e. the leaching process is slower when the periodic exchanges of solution are considered. One explanation is that calcium progressively increases in the ingressing solution, thus decreasing the calcium gradients and the corresponding fluxes towards the solution. A second one seems that the flux sign inverts (for the higher Na_2SO_4 solution) due to a decrease of calcium concentration in the material in the vicinity of its surface, and part of the leached calcium migrates in the specimen. This effect may be avoided by changing more frequently the ingressing solution.

The Fig. 14 presents the pH profiles. We observe that the pH, which is initially equal to about 7.35 in the Na_2SO_4 solution, rapidly increases in the first 7 days (first Na_2SO_4 solution) to reach about 12.67. This calculated increase is similar to the measured increase of pH from 6.2 to approx. 12.6 within 7 days reported by Brown [41] for OPC mortar samples submersed in 0.2 M Na_2SO_4 (28 g/l Na_2SO_4) solutions. At the end of the following cycles, just before the solution is exchanged, the pH reaches about 12.6.

These results suggest that the Na_2SO_4 solutions and their periodic changes have to be modelled in order to accurately simulate the degradation of cementitious material samples. Indeed, the concentrations of different species such as calcium vary significantly in the Na_2SO_4 solutions where the samples are immersed. These non-constant boundary conditions affect the chemical equilibrium in the samples, especially near the surface, and influence the mineralogical profiles, as described in Section 4.4.1. In particular, hydrates (gypsum, portlandite) exhibit non-smooth concentrations in the most degraded region, and due to the relatively high concentration of calcium in the Na_2SO_4 solutions on average, leaching is not complete in the outermost layer as attested by the presence of ettringite.

To which extent the exchange of the sulfate solution affects not only the amount of solids near the surface of the specimen but also the expansion is difficult to assess. The sulfate concentration and the pH of the solution and its changes with time have been observed to affect the expansion and the deterioration [41–44]. Low pH values generally lowers expansion as leaching becomes the dominant degradation mechanism [42]. The exchange of sodium sulfate solution during the measurements seems also to lower expansion [44], which might also be due to an increased leaching of the cement.

4.5. Comparison thermodynamic modelling — coupled chemical–transport modelling

Generally both modelling approaches gave comparable results. Some minor differences, however, were found which can be attributed to the different modelling approaches. In the simple thermodynamic model calculated with GEMS, the ingress of Na_2SO_4 solutions is mimicked by assuming that the mortar was in contact

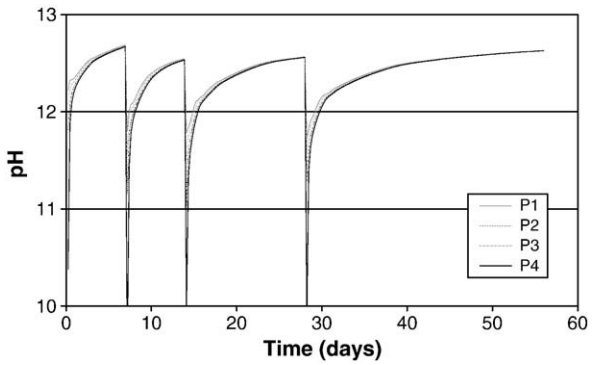

Fig. 14. Time evolution of the pH in the solution for the 44 g/l Na_2SO_4 case as obtained with ALLIANCES, for the points P1, P2, P3 and P4 located at 0.5, 4.0, 8.0 and 15.8 mm from the specimen surface.

with increasing concentrations of Na_2SO_4 solutions, while ALLIANCES coupled thermodynamic modelling with multi-species chemical transport calculations. The numerical results led to the following comments:

- Both numerical approaches gave the same trends regarding ingress of sodium sulfate solutions into mortars. GEMS provided fast results within 1 min, whereas ALLIANCES needed 1 to 5 days for the simulations but the results described the spatial and temporal degradation realistically.
- Gypsum precipitation was calculated in both modelling approaches for the higher Na_2SO_4 concentration. Portlandite and AFm were transformed into ettringite near the specimen surface. No SiO_2 was predicted.
- The SO_3 profiles obtained numerically by GEMS and by ALLIANCES showed the same trends and the calculated weight fractions agreed well.
- The ion concentrations in the samples appeared significantly affected by the composition of the Na_2SO_4 solution. Whereas K and OH showed a significant decrease between the core and the surface of the specimens, sulfate exhibited the same trend from the surface up to the degradation depth due to the precipitation of ettringite. There were some differences between the concentrations calculated by GEMS and by ALLIANCE. While the GEMS calculations seemed to indicate that K concentrations in the core of the sample remained high (and Na low), ALLIANCES was able to show clearly that a relatively fast leaching of K and ingress of Na has occurred. The concentrations of K and Na affected also the concentrations of the other elements and the pH. These differences in the calculated composition of the pore solution, however, had in the case studied no significant influence on the composition of the hydrate assemblage.
- Both modelling approaches were found to be well suited to calculate the chemical changes in the solid phases and the changes in volume associated with the ingress of sulfate (and sodium) in the mortar samples. The composition of the pore solution, however, is better represented by using transport modelling.
- It appears that the periodic exchanges of the Na_2SO_4 solution affected the mineralogical profiles. In particular, the calcium concentrations simulated by ALLIANCES reached values as high as 8.5 mmol/L near the surface (see Fig. 13) and were strongly affected by the frequency of the exchange of solution. With each exchange, calcium concentrations decreased in the solution and calcium was leached again from the sample due to the increased gradient. This suggests that frequent exchanges will lead to a stronger leaching of calcium compared to samples where the solution is not exchanged.

4.6. Comparison experimental results - modelling

The experimental findings were supported by the modelling results from GEMS or ALLIANCES, i.e. the instability of AFm phases and portlandite near the surface of samples stored in sodium sulfate solutions, the formation of ettringite (and gypsum) near the surface and the leaching of Ca from the C–S–H. The calculated changes of SO_3 and CaO were in agreement with the observed changes in the solid phases and the calculated weight fractions agreed relatively well with experimental data. The prediction of the depth of sulfate ingress at a specific time however, was not completely satisfactorily. The degradation depth predicted by ALLIANCES was greater for higher Na_2SO_4 concentration after 56 days than for the lower Na_2SO_4 concentration, as the higher concentration gradients led to a faster diffusion in the solid matrix and as less of the more concentrated solution was needed to completely transform the AFm phases into AFt. This very pronounced deeper penetration of sulfate at higher sulfate concentration after 56 days was not observed in the experimental results (Fig. 3 and Fig. 11), where a similar penetration of SO_3 ingress and CaO leaching in the 4 and 44 g/L Na_2SO_4 solutions was found. This disagreement may be explained by an inaccurate estimation of the diffusivity in the degraded zone of the specimens.

Thermodynamic modelling coupled with transport modelling offers a detailed description of the process through dissolution–precipitation reactions coupled to transport of ions in cementitious matrix. The complexity of the problem is increased by the fact that concrete structures in contact with a sulfate-bearing solution can not only be subjected to sulfate attack but are also usually affected by decalcification. The transport model used in this paper was able to reproduce the sulfate distribution across the sample and the distribution of the other solid phases. The results of the modelling presented in this paper are comparable to other transport modelling approaches reported in the literature [2,45,46]. Simulations of the chemical degradation by sodium sulfate solutions have been presented e.g. by Maltais et al. [2]. As in the present paper, the modelling of the penetration of sodium sulfate ions led to the formation of a layer of ettringite and gypsum at the vicinity of the exposed surface and to a distinct decalcification.

While such numerical models have the potential to describe the changes associated with the ingress of sodium sulfate solutions, they are not able per se to predict the mechanical consequences of sulfate ingress. Such transport models, however, can be coupled to mechanical models where the effects of macroscopic expansions due to ettringite formation and crystallization pressures can be considered (see e.g. [15,16,47]). The calculated total volume of the solids upon sulfate ingress exceeded for the cement studied in no case the initial volume of the paste. This indicates that it was not the overall volume restriction that led to the expansion but rather the formation of ettringite within the matrix and the consequent development of crystallisation pressures in small pores in the hydrated cement matrix. Whether and to which extent the total volume of the hydrates exceeds the initial volume of the paste depends on the chemical composition of the cement; especially for high C_3A cements where potentially large quantities of ettringite can be formed, the total volume of the hydrates is expected to exceed the initial volume of the paste.

5. Conclusions

The interaction of mortar with solutions containing sulfate led to the formation of a reaction front within the porous material. In regions near the surface, ettringite as well as gypsum (in the presence of high sulfate concentrations) precipitated. Further, within the sample the depletion of portlandite as well as the transformation of the AFm phases into ettringite was observed. High sulfate concentrations, as generally used in tests, led to the precipitation of ettringite and gypsum and to significant accumulation of SO_3 near the surface of the sample, while lower sulfate concentrations, as present under field conditions, led to ettringite but to no gypsum precipitation and to a less distinct accumulation of SO_3 near the surface. It should be noted that the presence of concentrated sodium sulfate solutions resulted not only in the precipitation of gypsum, but accelerated the ingress of sulfate and affected also the concentration of dissolved ions, as indicated by modelling.

Even test solutions containing lower sodium sulfate concentrations are significantly different from solutions predominant under field conditions, where a number of other cations such as potassium, calcium and magnesium and anions, mainly bicarbonate, will also be present. The occurrence of bicarbonate in sulfate containing solutions lowers the expansion very strongly as recently shown experimentally [5].

Periodic exchange of the Na_2SO_4 solutions, as prescribed for most sulfate tests, affects strongly the composition of the solution as with each renewal the sodium and sulfate concentration increase while the pH decreases. Frequent exchanges lead to a stronger leaching of calcium compared to samples where the solution is not exchanged. Under field conditions, where the sulfate containing solutions can

flow continuously, leaching will be even stronger (Fig. 10). The exchange has also a non-negligible effect on the mineralogical profiles and might also affect expansion [44].

Both modelling approaches give comparable results. While the pure thermodynamic modelling with GEMS provides fast results and the parameters are easy to vary, the results given by the coupled chemical–transport modelling with ALLIANCES offer additional information in terms of degradation depth and timescale. The same sequence of phases was observed in both modelling approaches and in the experimental results. Calculated and measured SO_3 and CaO profile in the solid phases agreed relatively well. Only the prediction of the progress of the sulfate front as function of the concentration of the sodium sulfate solution and time proved difficult with the coupled chemical–transport model. This aspect may be improved by a better estimation of the diffusivity in the zone of the material which is progressively degraded, and also by considering a distinct diffusivity for each ionic species. Moreover, taking into account kinetics in the formation of some minerals may reveal appropriate, in particular for ettringite. It could in addition explain the development of crystallization pressures (see e.g. [15]).

Thermodynamic models, whether coupled to transport models or not, are valuable tools to calculate the kind and amount of new phases formed and the changes in the volume of the solids caused by the ingress of sodium sulfate solutions. The comparison of experimental and modelling results supports interpretations and allows identifying critical parameters. Although both ettringite and gypsum precipitation tends to reduce the calculated porosity in the zones where portlandite is not totally dissolved (Fig. 5 and Fig. 9), the porosity in the mortar investigated was never totally filled. This indicates that for the sample studied, it was not the overall volume restriction that led to the observed expansion but rather the formation of ettringite within the matrix and the consequent development of crystallisation pressure in small pores in the hydrated cement matrix.

Acknowledgements

The financial support to Thomas Schmidt by cemsuisse is gratefully acknowledged. Thanks to Fred Glasser and Thomas Matschei, who gave very helpful insights into the modelling of sulfate ingress by simple thermodynamic models and to Wolfgang Kunther, Andres Idiart and Andreas Leemann for the helpful discussions.

References

[1] D. Planel, J. Sercombe, P. Le Bescop, F. Adenot, J.M. Torrenti, Long-term performance of cement paste during combined calcium leaching-sulfate attack: kinetics and size effect, Cement Concr. Res. 36 (2006) 137–143.
[2] Y. Maltais, E. Samson, J. Marchand, Predicting the durability of Portland cement systems in aggressive environments-laboratoy validation, Cement Concr. Res. 34 (9) (2004) 1579–1589.
[3] T. Schmidt, B. Lothenbach, M. Romer, J. Neuenschwander, K.L. Scrivener, Physical and microstructural aspects of sulfate attack on ordinary and limestone blended Portland cements, Cement Concr. Res. 39 (12) (2009) 1111–1121.
[4] F.P. Glasser, The thermodynamics of attack on Portland cement with special reference to sulfate, in: M.G. Alexander, A. Bertron (Eds.), Proc Concrete in Aggressive Aqueous Environments, Performance, Testing amd Modeling, Toulouse, France, RILEM, 1, June 3-5 2009, pp. 3–17.
[5] W. Kunther, B. Lothenbach, K. Scrivener, Influence of carbonate in sulfate environments, in: M.G. Alexander, A. Bertron (Eds.), Proc Concrete in Aggressive Aqueous Environments, Performance, Testing amd Modeling, Toulouse, France, RILEM, 2, June 3-5 2009, pp. 498–499.
[6] VAB-Ringversuch: Sulfatwiderstand nach SIA 262/1 Anhang D, VAB Report 024-06.06a, Vereinigung akkreditierter Baustoffprüflabors VAB/ALA, Beinwil am See, Switzerland, 2007.
[7] G. Moir, Sulfate resistance — state of the art, Report of the committee CEN/TC 51 N 865, Institute Belgie de normalisation, Bruxelles, Belgium, 2006.
[8] J. Marchand, E. Samson, Y. Maltais, J.J. Beaudoin, Theoretical analysis of the effect of weak sodium sulfate solutions on the durability of concrete, Cement Concr. Compos. 24 (3–4) (2002) 317–329.
[9] F. Adenot, M. Buil, Modelling of the corrosion of the cement paste by deionized water, Cement Concr. Res. 22 (2–3) (1992) 489–496.
[10] Y. Maltais, E. Samson, J. Marchand, Predicting the durability of Portland cement systems in aggressive environments — laboratory validation, Cement Concr. Res. 34 (9) (2004) 1579–1589.
[11] L. De Windt, D. Pellegrini, J. van der Lee, Coupled modeling of cement/claystone interactions and radionuclide migration, J. Contam. Hydrol. 68 (3–4) (2004) 165–182.
[12] M. Moranville, S. Kamali, E. Guillon, Physicochemical equilibria of cement-based materials in aggressive environments — experiment and modeling, Cement Concr. Res. 34 (9) (2004) 1569–1578.
[13] D. Planel, Les effets couplés de la précipitation d'espèces secondaires sur le comportement mécanique et la dégradation chimique des bétons. Thesis Université de Marne la Vallée, 2002.
[14] B. Bary, P. Le Bescop, Simplified chemo-transfer modeling of carbonation and sulfate attack in saturated cement pastes, Proc WCCM VI Beijing, China, Sept. 5-10 2004, Tsinghua University Press & Springer-Verlag, 2004, II n°408.
[15] B. Bary, Simplified coupled chemo-mechanical modeling of cement pastes behavior subjected to combined leaching and external sulfate attack, Int. J. Numer. Anal. Meth. Geomech. 32 (14) (2008) 1791–1816.
[16] R. Tixier, B. Mobasher, Modeling of damage in cement-based materials subjected to external sulfate attack. I: Formulation, J. Mater. Civ. Eng. 15 (4) (2003) 305–313.
[17] A. Franke, Bestimmung von Calciumoxid und Calciumhydroxid neben wasserfreiem und wasserhaltigem Calciumsilikat, Z. Anorg. Allg. Chemie. 247 (1941) 180–184.
[18] D. Kulik, GEMS-PSI 2.3, PSI-Villigen, Switzerland, 2009, available at http://gems.web.psi.ch/.
[19] T. Thoenen, D. Kulik, Nagra/PSI chemical thermodynamic database 01/01 for the GEM-Selektor (V.2-PSI) geochemical modeling code, TM-44-02-09, PSI, Villigen; available at http://gems.web.psi.ch/doc/pdf/TM-44-03-04-web.pdf, 2003.
[20] W. Hummel, U. Berner, E. Curti, F.J. Pearson, T. Thoenen, Nagra/PSI Chemical Thermodynamic Data Base 01/01, Universal Publishers/uPUBLISH.com, USA, also published as Nagra Technical Report NTB 02-16, Wettingen, Switzerland, 2002.
[21] B. Lothenbach, T. Matschei, G. Möschner, F.P. Glasser, Thermodynamic modelling of the effect of temperature on the hydration and porosity of Portland cement, Cement Concr. Res. 38 (1) (2008) 1–18.
[22] L.J. Parrot, Modeling of hydration reactions and concrete properties, in: J.P. Skalny (Ed.), Materials Science of Concrete, Westerville, OH, American Ceramic Society, 1989, pp. 181–195.
[23] G.J. Verbeck, R.H. Helmuth, Structure and physical properties of cement paste, Proc. 5th Int. Symp. Chem. Cem. Tokyo III (1968) 1–32.
[24] J.J. Thomas, H.M. Jennings, A colloidal interpretation of chemical aging of the C–S–H gel and its effects on the properties of cement paste, Cement Concr. Res. 36 (1) (2006) 30–38.
[25] L.J. Parrot, D.C. Killoh, Prediction of cement hydration, Br. Ceram. Proc. 35 (1984) 41–53.
[26] L.J. Parrot, Modelling the development of microstructure, Proc Research on the manufacture and use of cements, Henniker NH, Engineering Foundation, New York, 1986, pp. 43–73.
[27] B. Lothenbach, G. Le Saout, E. Gallucci, K. Scrivener, Influence of limestone on the hydration of Portland cements, Cement Concr. Res. 38 (6) (2008) 848–860.
[28] B. Lothenbach, F. Winnefeld, Thermodynamic modelling of the hydration of Portland cement, Cement Concr. Res. 36 (2) (2006) 209–226.
[29] J. van der Lee, L. de Windt, Chess tutorial and Cookbook, updated for version 3.0, in, ENSMP-CIG LHM/RD/02/13, 2002.
[30] J. van der Lee, L. De Windt, V. Lagneau, P. Goblet, Module-oriented modeling of reactive transport with HYTEC, Comput. Geosci. 29 (3) (2003) 265–275.
[31] G.T. Yeh, V.S. Tripathi, A critical evaluation of recent developments in hydrogeochimical transport models of reactive multichemical components, Water Resour. Res. 25 (1) (1989) 93–108.
[32] E. Nozourtier-Mazauric, Prise en compte des variations de porosité dans le couplage transport-chimie mis en œuvre dans ALLIANCES Note technique CEA, 2004.
[33] E. Stora, B. Bary, Q.C. He, On estimating the effective diffusive properties of hardened cement pastes, Transp. Porous Med. 73 (3) (2008) 279–295.
[34] E. Stora, B. Bary, Q.C. He, Modelling and simulations of the chemo-mechanical behaviour of leached cement-based materials. Leaching process and induced loss of stiffness, Cement Concr. Res. 39 (9) (2009) 763–772.
[35] T. Schmidt, Sulfate attack and the role of internal carbonate on the formation of thaumasite. Thesis EPFL, Lausanne, Switzerland, 2007.
[36] E.F. Irassar, V.L. Bonavetti, M. González, Microstructural study of sulfate attack on ordinary and limestone Portland cements at ambient temperature, Cement Concr. Res. 33 (2003) 31–41.
[37] P. Le Bescop, C. Solet, External sulphate attack by ground water. Experimental study on CEM I cement pastes, Revue européenne de Génie civil 10 (9) (2006) 1127–1145.
[38] C.F. Ferraris, P. Stutzman, M. Peltz, J. Winpigler, Developing a more rapid test to assess sulfate resistance of hydraulic cements, J. Res. Natl Institute of Stand. Technol. 110 (2005) 529–540.
[39] G.W. Scherer, Stress from crystallization of salt, Cement Concr. Res. 34 (2004) 1613–1624.
[40] B. Lothenbach, E. Wieland, A thermodynamic approach to the hydration of sulphate-resisting Portland cement, Waste Manag. 26 (7) (2006) 706–719.
[41] P.W. Brown, An evaluation of the sulfate resistance of cements in a controlled environment, Cement Concr. Res. 11 (1981) 719–727.
[42] H.T. Cao, L. Bucea, A. Ray, S. Yozghatlian, The effect of cement composition and pH of environment on sulfate resistance of Portland cements and blended cements, Cement Concr. Comp. 19 (2) (1997) 161–171.
[43] R.P. Kathri, V. Sirivivatnanon, J.L. Yang, Role of permeability in sulphate attack, Cement Concr. Res. 27 (8) (1997) 1179–1189.

[44] C.F. Ferraris, J.R. Clifton, P.E. Stutzman, E.J. Garboczi, Mechanisms of degradation of Portland cement-based systems by sulfate attack, in: K.L. Scrivener, J.F. Young (Eds.), Mechanisms of Chemical Degradation of Cement-based systems, E & FN Spon, London, 1997, pp. 185–192.
[45] F.P. Glasser, J. Marchand, E. Samson, Durability of concrete — degradation phenomena involving detrimental chemical reactions, Cement Concr. Res. 38 (2) (2008) 226–246.
[46] J. Marchand, E. Samson, Y. Maltais, J.J. Beaudoin, Theoretical analysis of the effect of weak sodium sulfate solutions on the durability of concrete, Cement Concr. Comp. 24 (3–4) (2002) 317–329.
[47] M. Basista, W. Weglewski, Chemically assisted damage of concrete: a model of expansion under external sulfate attack, Int. J. Damage Mech. 18 (2) (2009) 155–175.
[48] E. Corazza, C. Sabelli, The crystal structure of syngenite, $K_2Ca(SO_4)_2H_2O$, Z. Kristallogr. 124 (1967) 398–408.